Supplementary material

Part A: *Material and Methods for physical and biogeochemical parameters*

Temperature (T) and conductivity depth profiles were performed at each cast with a CTD SBE 911plus mounted on a Carrousel Sea-Bird SBE 32 sampler of 24, 12-liter Niskin bottles. Sensors were scanned at 24 Hz with the Seasave Win32 V 5.37m software, and were namely : Digiquartz (0-6000) for pressure, two lots of SBE-3S and SBE 4C for T and conductivity, one oxygen sensor SBE43, one transmissometer SeaTech (wavelength 660 nm, 25-cm path length) for light attenuation coefficient (c), one fluorimeter Chelsea configured on Chl a measurements, surface PAR and underwater PAR for light measurements (Biospherical), ISUS (SAtlantic) for nitrate measurements, and a pinger to measure the distance to bottom and approach it with less than 5 meters, with a maximum depth reached of 3020 dbars due to sensor limitations.

All data were processed with the software "Seadata processing" of Seabird after post-cruise calibrations for T and conductivity sensors by Seabird. The processing ended after calculations of salinity (S), T, potential T (θ), density (σ_θ), dissolved oxygen concentration (O_2), Fchla, by a bin average for each at one meter.

Final accuracies were estimated to be 0.001°C for temperature (ITS90), 0.002 for S (PSS78), 2 µM for O_2 following calibration against Winkler sampling data. ISUS nitrate profiles (limited to 500 dbars) were very noisy and used following calibration against nitrate bottle data measurements to obtain nitracline depths only.

Transmissiometer data, obtained with a Seapoint transmissiometer with a 25 cm optical length in seawater, were processed to give the beam attenuation coefficient, c(660), for sea water, expressed in m^{-1}. In order to get the attenuation coefficient for suspended particles, Cp(660), the contribution from pure seawater has to be subtracted to c(660). Instead of using a calibration factor, the mean c(660) value measured between 350 and 400 m was subtracted from each profile since at these depths, the very low particle concentration induces c(660) values very close to the value for particle-free water (Loisel et al., 2011).

RDI VMADCP 75kHzNB data were processed from raw data averaged every 2 minutes, with bins of 16 m from 29.5 m down to around 600 m; using GPS navigation and laboratory

processing (L. Prieur) in order to screen out bad data and to correct (weak, in order 0.5 deg.) misalignment between earth referential and ADCP axes.

MLD estimations and biogeochemical parameters

Three mixed layer depths ($MLD_{0.03}$, MLD_{2d}, W-MLD) were obtained from the same vertical density profile, $\rho(z)$ at time t_p, having a 1 dbars resolution (Table 1). $MLD_{0.03}$ was calculated considering the standard criterion of depth where density equals surface density + 0.03 kg m^{-3}. The two other mixed layer depths were predictions of the deeper mixed layer depths estimated between a previous initial time t_i and t_p; t_i = 3 days (MLD_{2d}) or t_i = 200 days (W-MLD) before the time t_p of the density profile measurement (see supplementary material). The three MLD were calculated from the first cast at each SD station and from the last CTD cast at each LD station, A, B and C. W-MLD corresponds to the maximum mixing depth that would have been measured during winter 2008, before the summer 2008 BOUM cruise.

The Euphotic Zone Depth (EZD, dbars) was estimated according to Morel and Maritorena (2001) from the discrete profiles of chlo a measurements and measured at depth where I = 0,01 surface PAR (Table 1).

The Deep Chlorophyll Maximum Depth (DCMD, m) is the depth where in vivo fluorescence sensor CTD reaches a maximum value. Fluorescence Units were converted into total chlorophyll a (Tchlo a) concentration using the best fit linear relationship between the Fluorescence Units and total chlorophyll a as measured by HPLC (r^2 = 0.98, N = 79). Integrated total chlo a concentration (Ichlo a, mg m^{-2}) was calculated between 0-150 dbars (for bottom depth < 150 dbars, the integration was performed from 0 to bottom depth minus 6 dbars).

Nutrient measurements are detailed in Pujo-Pay et al. (2011). Characteristics of nutriclines (Table 1) were calculated according to Moutin and Raimbault (2002) for nitrate (NO_3) and phosphate (PO_4), respectively, with D_x (m) = the depth at which NO_3 or PO_4 reaches zero, S_x (nM m^{-1}) = the slopes of the regression lines between concentration and depth (related to nutrient consumption, i.e. globally related to the EZD and calculated when a significant linear relationship was obtained between nitrate or phosphate concentration plotted against depth at the depths of the nutricline), N_x = number of samples and r_x^2 = correlation coefficient). All 0-500 m CTD casts were considered for the calculations at the LD stations. The depths before (°) and after (+) a large (> 100 h) increase in phosphate turnover time ($DTPO_4$) are calculated

(see Moutin et al. (2002) for a detailed description of the methodology used for phosphate turnover time measurements with ^{33}P). Integrated nitrate and phosphate concentrations (INO_3 and IPO_4, mmol m^{-2}) were calculated between 0-150 dbars.

Primary production and integrated primary production were measured and calculated according to Moutin and Raimbault (2002) allowing a direct comparison with previous cruise (MINOS, BIOSOPE) data in oligotrophic areas.

Oxygen solubility was calculated using Benson and Krause (1994) algorithm.

Part B: ***LTMLD –Lagged Time Mixed Layer Depth - Method***

This method uses a vertical density profile, ρ(z), at a given date and time (t_p), and net surface heat and water fluxes at the same geographical position, together with a specific window of time *win* before the date of the density profile (t_p). Surface buoyancy fluxes are calculated using:

$$J_b = g\ \alpha Q_{net}/(\rho_s C_p) + g\ SSS\ \beta Q_e /(\rho_s L_v)$$

where J_b is the buoyancy flux (in $m^2 s^{-3}$) from the atmosphere to the ocean, Q_{net} and Q_e are, respectively, the net heat and water fluxes modifying salinity (in W m^{-2}), ρ_s is surface water density, *SSS* is sea surface salinity, C_p and L_v are specific heat capacity and latent heat coefficients, and g is the gravity acceleration (Gill, 1982; D'Ortenzio and Prieur, 2012). The terms α and β are the thermal and the salinity expansion coefficients for seawater, and are represented by:

$$\alpha = -\ (1/\rho_s)\ \partial\rho_s/\partial SST$$

$$\beta = \ (1/\rho_s)\ \partial\rho_s/\partial SSS$$

where *SST* is the sea surface temperature (°C) and *SSS* the sea surface salinity (PSU). The time window *win* $[t_i, t_p]$ before the observation time t_p is fixed, where t_i is anterior to t_p. For example, t_i could be chosen as t_p-1 day, or t_p- 3 days so that *win* encompasses some anticipated maximum MLD for 1 or 3 days before t_p, or even t_p-200 days when the aim is to retrieve maximum Winter MLD several months before t_p.

The temporally cumulated surface buoyancy flux [cumJb(t)] for *win* is then calculated, and the time (t_m), the value of cumJb(t_m), of minimum cumJb(t) inside the temporal window, and cumJb(tp) are found.

BI(z) is the vertical profile of integrated buoyancy from the profile of ρ(z) at time t_p, which is calculated for any depth -h as follows :

$$BI(h) = \left(g / \rho 0 \right) . \int_{-h}^{0} (\rho(h) - \rho(z)) dz$$

where ρ0 is any constant density reference near the density range of ρ(z). BI is the buoyancy integral of the measured buoyancy profile.

The LTMLD (t_m, t_p) value is obtained from the equation:

$$BI(LTMLD) = cumJb(t_p) - cumJB(t_m),$$

where LTMLD is the lagged time mixed layer depth. This equation states that the amount of excess buoyancy brought by the atmosphere since time t_m down to the ocean has increased the oceanic buoyancy content at the location of the measured density profile. BI(LTMLD) corresponds to this amount, on condition, however, that advection of buoyancy is negligible for the time window *win*.

The above procedure proceeds with a retrograde window (i.e. $t_i < t_p$).

In the particular case where LTMLD is sought for a time after the date of the profile (prograde), *win* is chosen as the temporal window [t_p,t_i], which means that the excess buoyancy contained in the ocean at t_p is lost through the atmosphere because of the accumulation of negative Jb between t_p and t_m. In both prograde and retrograde cases, the vertical profile ρ(z) observed at time t_p is more buoyant than one which might have been observable at time t_m.

Since density increases with depth, BI(h) is always positive. Thus, the depth profile will be more 'buoyant' at t_m than at t_p, and so the ocean becomes stratified or unstratified during the period [t_m, t_p].

However, the value found for LTMLD cannot be the real, value that might have been observable at time t_m, because the method does not take into account changes in density profiles due to advection. Nevertheless, use of this method has been found to give realistic

values of MLD (Prieur et al., 2010). In Figure 7, the winter mixed layer depths (W-MLD) in 2008 were calculated with a window of 200 days using ECMWF surface fluxes for each cast of the section. Indeed, the W-MLDs found correspond very closely to the top depth of the nutricline and were deeper for casts inside the eddies than for those outside. The W-MLD was also fairly close to the depth where AOU is nil or weak. This can be interpreted as one indication of winter ventilation of depths less than W-MLD and with a positive net production for the *win* period. At depths above W-MLD, the net production is negative and AOU starts to increase with depth.

MLD_{2d} has another signification, which is to define the maximum mixing depth that might have been measured in a time window of 3 days before the measurement (t_p – 3days, t_p). Indeed, MLD_{2d} values were similar to the maximum $MLD_{0.03}$ values measured every 3 hours during LD station occupation, given that the MLD_{2d} method was applied for the last cast of each LD station A, B and C.

This work was funded by Mercator-Coriolis PROSAT Grant n° Ifremer 08/ 2 210 118

Part C: *Simulation of an eddy*

The objectives are to specify the fitting method used to simulate observed eddy structure during the BOUM experiment through use of an idealized structure, to show some of the characteristics and dynamical properties of the eddies, and to evaluate the quality of the fit by comparing observed and simulated fields particular to eddy A.

Dynamical characteristics of a typical anticylonic eddy

A surface intensified mesoscale eddy in an ocean in rotation (f>0 in the northern hemisphere) shows the following dynamical properties (Defant, 1961) : Geopotential differences “in” – “out” ($\delta G(z)$) is >0, azimuthal velocity (Vaz) is <0 at any depth, and the difference of the transport function (F) between the two casts is locally maximum. These specific characteristics are observed for the three studied eddies (Table 2 and Fig. 7, see also supplementary material). The isopycnal lines deepen (see ΔH, Table 2 and Fig. SM2 bottom) towards the eddy centre, at least when Vaz is decreasing with depth. When negative Vaz is increasing with decreasing depth, the isopycnal slope is reversed (see Fig. 4 in McGillicuddy

et al., 1999, mode water eddy case), as was observed close to the surface in our eddies. In this case, the maximal absolute velocity Vaz_{Max} occurs not at surface but at a depth $DVaz_{Max}$ below the surface and at a horizontal distance ½ $rVaz_{Max}$ from the eddy axis. Due to the deepening of the isopycnal lines, the vertical spacing of isopycnals increases and the square of the Brunt Vaïssala frequency ($N^2=-g/\rho.\partial\sigma/\partial z$) decreases near to the axis. Hence, a pycnostad appears on the "in" density profile. At depths greater than the depth of maximum σ anomaly, N^2 for the "in" profile is higher than for the "out" profile because at great depths, density is the same for both profiles. In addition, as the relative vorticity ζ calculated as $2\omega/f$ is negative near the axis for an anticyclonic eddy, the absolute potential vorticity (Gill, 1982) near the axis is $fN^2/g(1+\zeta/f)$ and less than the same for "out" profile. It is due firstly to N^2 and secondly to the negative value of ζ. Thus, the inner part of an eddy is characterized by a trough of absolute potential vorticity which isolates the eddy core in solid rotation from any outer advection. The horizontal limits of this trough are given in supplementary material. When the eddy rotation velocity is sufficiently high, a pycnostad with a nil vertical gradient occurs when $|\zeta| = f$. This may happen during eddy formation, particularly in winter (Brenner et al., 1991). However, in spring and summer, the top of the eddy is warmed and some geostrophic adjustments occur. As a consequence, the vertical density gradient in the eddy core is not nil but keeps a lower value than outside the eddy (Chapman and Nof, 1988) and the eddy takes the shape of a mode water eddy (Pingree and Le Cann, 1992; McGilliccudy et al., 1999), and the winter time mixed layer depth (as estimated from W-MLD, Table 1) is greater "in" than at the corresponding "out" station. The water body was more recently in contact with the atmosphere and therefore more oxygenated inside the eddy. This is the reason why an anomaly of AOU corresponds to anomalies in σ, θ, and S.

Horizontal anomalies are conserved inside the body of water around the axis because it is isolated from mixing and advection from surrounding waters during the life time of the eddy. This is due to the strong influence of ζ on potential vorticity conservation (see supplementary material treating the shape of such a body of water). Thus, the so-called anomalies are typical properties of each eddy and are easy to observe from CTD casts. They also provide information about the period and location of the eddy formation. It is interesting to note (Table 2) that inferred ζ, <0, remains a sizeable fraction of f, roughly -0.3 to -0.4 f, and is of the same magnitude as that observed for meddies, smeddies or swoddies (Pingree and Le Cann 1992, 1993).

Eddy Equations

In cylindrical coordinates (r, φ, z), a circular, stationary, geostrophic eddy with vertical axis and velocity gradient ($v_r = 0$, v_φ, $v_z = 0$) satisfies the following equations (Brenner, 1993):

$$v_\varphi^2/r + f\, v_\varphi = (1/\rho_r)\, \partial p/\partial r = f v_g \qquad (1)$$

$$\partial p/\partial z = -g\, \rho(r,z) \qquad (2)$$

$$f \partial v_g/\partial z = -(1/\rho_r)\, \partial \rho/\partial r \qquad (3)$$

Equation (1) is the radial-moment equation, where f is the Coriolis parameter, p is pressure, v_g is geostrophic velocity and ρ_r is a constant reference density. The second equation in (1) states only the geostrophic equilibrium and shows that geostrophic velocity v_g is different from gradient velocity due to cyclostrophic acceleration. Equation (2) accounts for the use of hydrostatic approximation. Equation (3) is the conventional wind thermal equation which links velocity to density fields.

Other dynamical quantities are the vertical relative vorticity component ζ and Ertel potential vorticity Q, when the two horizontal components of vorticity are nil or negligible and N^2 is the Bünt Vaîssala frequency:

$$\zeta = (1/ r)\, \partial(r v_\varphi)/\partial r$$

$$Q = f\, N^2\, (1 + \zeta/f)/g$$

$$N^2 = -(g/\rho_r)\, \partial \rho/\partial z$$

A measurement of the non-linearity of an eddy is given by the standard Rossby number for eddies

Ro $= |\zeta_{min}|/f$. Ro typically ranges from 0.20 to 0.60 for coherent anticylonic vortex (Brenner, 1993, Pingree and Le Cann, 1992)

A simple analytical velocity $v_\varphi(r, L)$ summarizing an idealized structure for BOUM eddies is a Rayleigh distribution on a horizontal plane (Pingree and Le Cann, 1993).

$$v_\varphi = \omega\, r \exp(-r^2/L^2)\ ;\ v_r = 0\ ; \qquad (4)$$

where ω is rotation pulsation ($\omega = 2\pi/Tr$, Tr rotation period) and L is a distance, here called Rayleigh distance. ω is negative for an anticyclonic eddy in the Northern hemisphere.

$$\psi = -\omega(L^2/2)\exp(-r^2/L^2) \quad (5)$$

such as $v_\varphi = \partial\psi/\partial r$. ($\psi>0$ when $\omega<0$). Using a stream function ψ_g such as $v_g = \partial\psi_g/\partial r$ and a without dimension parameter ψ_{cor}, the combination of equations (1), (4) and (5) gives an expression for ψ_{cor}:

$$\psi_g = \psi.\psi_{cor} \quad (6)$$

$$\psi_{cor} = [1 + (\omega/2f)\exp(-r^2/L^2)] \quad (7)$$

Near to an anticyclonic eddy axis, $\psi_{cor} < 1$, and the geostrophic stream function is flatter than the gradient stream function. When r>>L, both are equal.

Figure SM1 shows an example of radial variations at z= constant of $f\psi$ (in black, Top panel) and $f\psi_g$ (red). The azimuthal velocity gradient (middle panel) is always negative, decreasing linearly as ωr to $r \sim L/3$, minimum at $r = L/\sqrt{2}$ and increases further towards 0. Relative vorticity scaled by f (bottom panel) is minimum near the axis and equal to $Ro = -\zeta/f$, then increases between r = 0 and r = L. Following this last r value, the relative vorticity is positive, reaches a maximum at $r = L\sqrt{2}$, and then decreases towards 0.

Table SM1 shows the numerical value for the different characteristic values of r scaled by L and corresponding Vaz (= v_φ) values scaled by ωL. Vo is hereafter defined as ωL for convenience.

Fitting an idealized structure to observed eddies

It is necessary to adjust ω and L in order to obtain a idealized 3D structure of an observed eddy. In the adjustment, ω is assumed to be constant with depth, and L variable, L=L(z).

Similar adjustments have already been applied, for example by Pingree and Le Cann (1993) who used geostrophic calculations and measured velocities from drogued buoys and/or VMADCP. An example of adjustment with the method proposed here is presented for eddy A. A complete eddy A work map is presented in Figure SM2 (Top). Locations of VMADCP measurements are indicated (blue line, see also Figure 8). As the depth ranges of correct horizontal velocity measurements were strongly variable, the ESE-WNW XBT section was used to compare simulated and observed Vaz. This section crosses the eddy approximately along a diameter and observations of the maximum radial velocity range 30-40 cm s^{-1} and

$|Vaz|_{max}$ was chosen as 33 cm s^{-1} at 60 m depth. A second sort of information from observations is the vertical profile of the geopotential difference $\delta G(z)$ between the cast near the centre of eddy (cast 147) and the outer cast 130. A South to North nine-cast CTD section A (marked in thick red in Figure SM2) was performed, starting with cast 147 the day following the XBT section described above and near to the presumed location of the eddy centre. This CTD section (A) was prolonged by a section at this northern tip in order to reach a virtual cast 130', at the same distance from eddy center (120 km) than cast 130. Data from cast 130 has been used at cast 130' assuming eddy circular axis symmetry.

The vertical density profiles for both casts 147 and 130 are seen superimposed in Figure SM2 (bottom), with vertical profiles of density anomaly and the $\delta G(z)$ profile calculated from T and S profiles. The maximum of $\delta G(z)$ was also observed at 60 m.

ω and L(z) were then calculated in 2 steps. First, ω was calculated and second, the profile of L(z) using 2 expressions was determined from equations (5), (6) and (7) :

at r=0 :

$$f\,\psi_g(r=0,z) = \delta G(z) = f\,\omega(L^2/2).[1+(\omega/2f)] , \qquad (8)$$

as $Vo = \omega L$:

$$fVo(z)L(z)[1+(Vo/2fL)] = \delta G(z) \qquad (8b)$$

and

$$Vo = -|Vaz|_{max}/0.429 \quad \text{at } z = \text{depth of } \max[\delta G(z)] \qquad (9)$$

Relation (9) is determined using Table SM1

step 1

For z= 60 m where $\delta G(z)$ and |Vaz| are maximum, let:

$V = -|Vaz|max$

$G = \max[\delta G(z)]$

ω is then calculated using equations (8) and (8b)

$Vo = V/0.429$; using table SM1 for $r = L/\sqrt{2}$

$L = -(1/fVo)[4G+Vo^2]/2$; using equation (8b)

$\omega = Vo/L$

step 2:

L(z) is calculated using found ω and equation (8).

Then, v_φ -using equation (4)- and ζ can be obtained at any r and z as can v_g using equation (1).

The simulated density field is required to calculate potential vorticity Q. This was achieved by using the "out" profile of cast 130 at r_o =130 km and a numerical horizontal integration from r_o to any r using equation (3). All numerical calculations were performed on a grid spacing of 2 km on r and 10 m on z.

Potential vorticity could then be calculated.

Results

Eddy A was simulated as described above with -1.8181 e-05 s^{-1}, which corresponds to Tr= 4 days using $\delta G(z)$ profile of Figure SM2 and G= 1.26 $m^2 s^{-2}$; f=9.1531e-05 s^{-1} ; V=- 32 cm s^{-1} at 60 m. The Rossby number Ro was found to be as high as 0.3973, which corresponds to a relatively high importance of cyclostrophy and the coherent vortex nature of Eddy A.

Figure SM3 shows along-diameter sections of idealized structure for azimuthal velocity (upper left, drawn as <0 when ingoing the figure and >0 when outgoing), σ_θ (upper right), ζ/f (bottom left) and absolute potential vorticity (Bottom right). For clarity, the section ranges from -70 to 70 km on the X-axis. On each graph can be seen the representative loci of maximum of absolute azimuthal velocity (dotted), and null and maximum relative vorticity (solid and dashed lines, respectively) . Isopycnal lines are seen to deepen toward the axis by approximately ΔH = 100 m for a range of σ_θ 28.2 -29 kg m^{-3}, but when looking at lower σ_θ, ΔH decreases and even changes sign near 50 m, where isopycnal 27.5 is flat, as anticipated from density profiles in Figure 2SM. In the narrow, 20-50 m depth range , the density in the eddy core is higher than it is outside. Such a feature has already been observed for deep anticylonic eddies as well as for meddies and also for swoddies (Pingree and Le Cann , 1992) and was theoretically explained by differential heating /cooling by Chapman and Nof (1988). The ζ/f graph also clearly shows the envelope of maximum relative vorticity which crosses through the density lines on σ_θ , thus forming a barrier of potential vorticity which separates the inner part of the eddy from the outer part horizontally and along the isopycnal, due to a maximum of Q.

Figure SM4 compares the azimuthal velocity field (left) and density field as they were observed (black isolines) superimposed upon the oxygen field (Top) and according to simulations (Bottom). On the right, only the radius sections which correspond to the observed section A have been drawn. Simulated and observed velocity sections show similar patterns, both for amplitude and depth, even if on observed ADCP sections some dissymmetry in maximum amplitude was noted. The differences remain minor (5-7cm s^{-1}) and can be explained by inertial internal waves, errors in ADCP velocities (circa +-2 cm s^{-1}), possible drifting of the eddy centre (2-5 cm s^{-1}) and by possible ringing of the eddy. The reconstitution is fairly close to what was observed. The deepening of isopycnals is also quite similar. The bigger, although still moderate, discrepancies appear from range 20-40 km to depth. However, the pycnostads 28.1-28.2 kg m^{-3} at 130-170 m and nearly 28.6 kg m^{-3} at 200-250 m are retrieved near the axis in the simulated field. In fact, the reconstituted and observed density profiles for r = 0 (not shown), are similar (difference less than 0.02 kg m^{-3}) due to the use of observed geopotentials in the procedure. This can be the case only when highly accurate $\delta G(z)$ is available.

The barrier effect of potential vorticity maximum is marked when looking at the observed oxygen field. Strong horizontal gradients are evidenced between solid and dashed lines, while outside of this slanting band the oxygen concentrations are quite homogeneous even if some vertical gradient can be noted. The core of the eddy is not a fully homogeneous body of water due to residual stratification, even if it is isolated from the outer part of the eddy. Some drawing discrepancies are visible and have been attributed to the interpolation method between the end of the real section A (at 55 km; real casts are marked by a white cross and the virtual cast 130).

Because the observed data fitted well with the idealized eddy structure, it was possible to determine the Rossby number, ζ/f, which is a characteristic number for each eddy. The Rossby number evidences the shape of the inner part of eddy A, isolated from the outer part. Comparable simulations were performed for eddies B and C. The first results are not as accurate as for eddy A, and are reported in Table 3. Recorded velocities at LD B and C by ADCP were lower than for eddy A, and the influences of internal near-inertial waves and drifting of eddy centres could have been greater. Future work is needed to optimize the fitting and to find more accurate ω by taking ARGO float trajectories and profiles for these eddies into account.

References (only those not already in the paper) :

Benson, B. B. and Krause, D.: The concentration and isotopic fractionation of oxygen dissolved in freshwater and seawater in equilibrium with the atmosphere, Limnl. Oceanogr., 29, 620–632, 1984.

Brenner, S., Rozentraub, Z., Bishop, J., and Krom, M.: The mixed layer/thermocline cyle of a persistent warm core eddy in the eatern Mediterranean, Dyn. Atmosph. Oceans, 15, 457-476, 1991.

Defant, A.: Physical Oceanography. Pergamon, New York, vol. 1, 729 pp., 1961.

Gill, A. E.: Atmosphere-Ocean Dynamics. Academic Press, 662 pp, 1982.

Loisel, H., Vantrepotte, V., Norkvist, K., Mériaux, X., Kheireddine, M., Ras, J., Pujo-Pay, M., Combet, Y., Leblanc, K., Dall'Olmo, G., Mauriac, R., Dessailly, D., and Moutin, T.: Characterization of the bio-optical anomaly and diurnal variability of particulate matter, as seen from scattering and backscattering coefficients, in ultra-oligotrophic eddies of the Mediterranean Sea, Biogeosciences, 8, 3295-3317, doi:10.5194/bg-8-3295-2011, 2011.

McGillicuddy D. J. Jr., Johnson R., Siegel D. A., Michaels A . F., Bates N. R., and Knap A. H.: Mesoscale variations of biogeochemical properties in the Sargasso Sea. J.Geophys.Res., vol. 104, C6, 13,381-13,394, 1999.

Pingree R. D., and Le Cann, B.: Anticyclonic Eddy X91 in the Southern Bay of Biscay, May 1991 to February 1992. J. Geophys. Res., 97, C11, 14353-14367, 1992.

Pingree R. D., and Le Cann, B.: A Shallow Meddy (A Smeddy) From the Secondary Mediterranean Salinity Maximum. J. Geophys. Res., 98, C11, 20169-20185, 1993.

Prieur, L., Caniaux, C., D'Ortenzio, F., Lavigne, H., and Giordani, H. : Etude de faisabilité de l'application de méthodes d'exploitation conjointe des séries de profils in situ et des séries d'images satellitaires aux fins de l'Océanographie Opérationnelle : Couche mélangée à partir des profils ARGO, Images satellitaires et flux de Surface. Rapport final de contrat Ifremer 08/ 2 210 118, 25 Octobre 2010. 55 pp., 2010.

Table SM1

	Solid limit Rsol	Max$\|V_{az}\|$ $R_{Vaz\ max}$	$\zeta = 0$ R_{core}	Max ζ R_{ζ}	 R_{tot}
r	0.333 L	0.707L	L	1.414L	2L
V_{az}	$0.333\omega L\ e^{-0.11}$	$0.707\omega L\ e^{-0.5}$	$\omega L\ e^{-1}$	$1.414\ \omega L\ e^{-2}$	$2\omega L\ e^{-4}$
V_{az}	0.299 ωL	0.429 ωL	0.378 ωL	0.1914 ωL	0.0366 ωL

Table SM1: Numerical values of different characteristic values of r scaled by L, and corresponding Vaz (= v_{φ}) values scaled by ωL using the Rayleigh model.

Figure captions :

Figure SM1: Examples of radial variations of $f\psi$ (red) and $f\psi_g$ (red) for a Rayleigh eddy simulation, using L = 25 km, Tr = 5.5 days (Top), azimuthal velocity Vaz (Middle) and ζ/f ratio (Bottom). The x-axis spans the 0-80 km range along an eddy radius. The 3 * on each graph marks the distances $L/\sqrt{2}$, L and $L\sqrt{2}$, where Vaz (<0) reaches an extremum, $\zeta = 0$ and ζ is maximum, respectively. Units are indicated in brackets in the titles.

Figure SM2: Map of work, eddy A (Top). The 4-day ship track between casts 130 and 187 is indicated as a solid blue line with dashed arrows. Numbers given refer to the cast numbers cited in the text. Pink lines correspond to section A with observed (thick) and prolonged (dashed) parts (see text). Bottom: from left to right, σ_θ, anomaly $\delta\sigma_\theta$ and $\delta G(z)$ respectively. On the left, a vertical black line indicates the isopycnal deepening ΔH of the density observed at the negative maximum of $\delta\sigma_\theta$ depth. Horizontal black dashed and solid lines, respectively, depict the top and bottom of density anomaly in the middle panel. The top of anomaly $\delta\sigma_\theta$ corresponds to the depth of a maximum of δG (right) and the intersection of the two σ_θ (z) (left).

Figure SM3: Eddy A, Rayleigh simulation.

Figure SM4: Comparison for eddy A between observed (Top) and simulated (Bottom) fields.

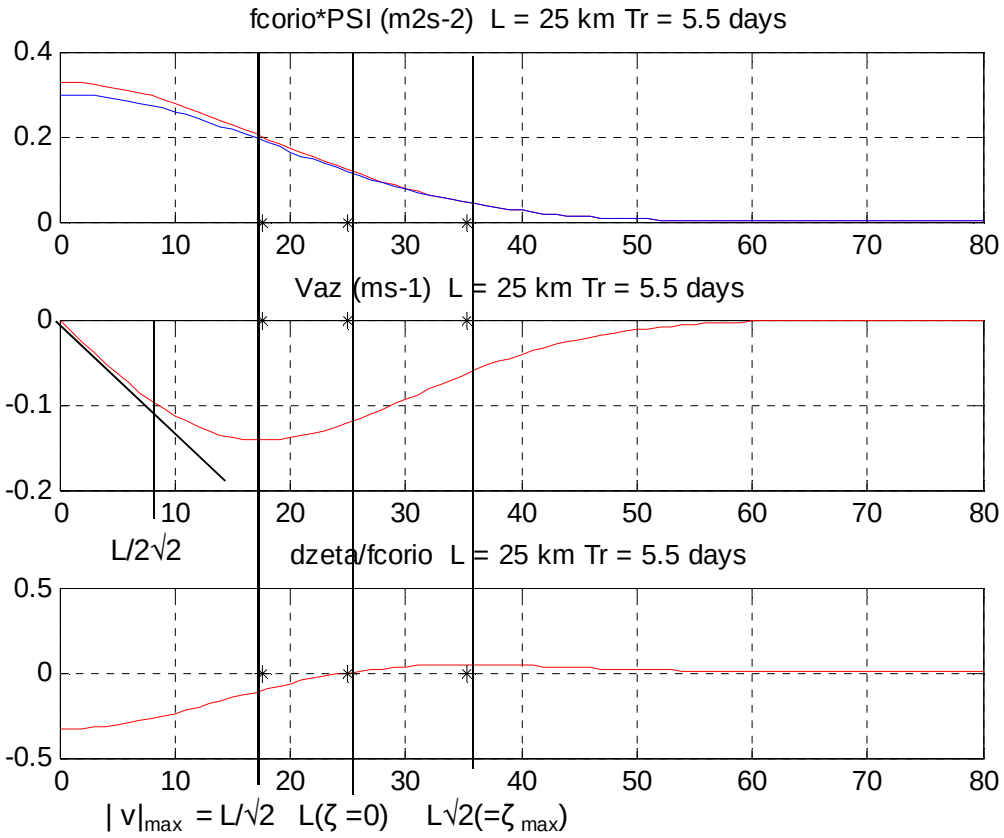

Fig. SM1 Moutin and Prieur

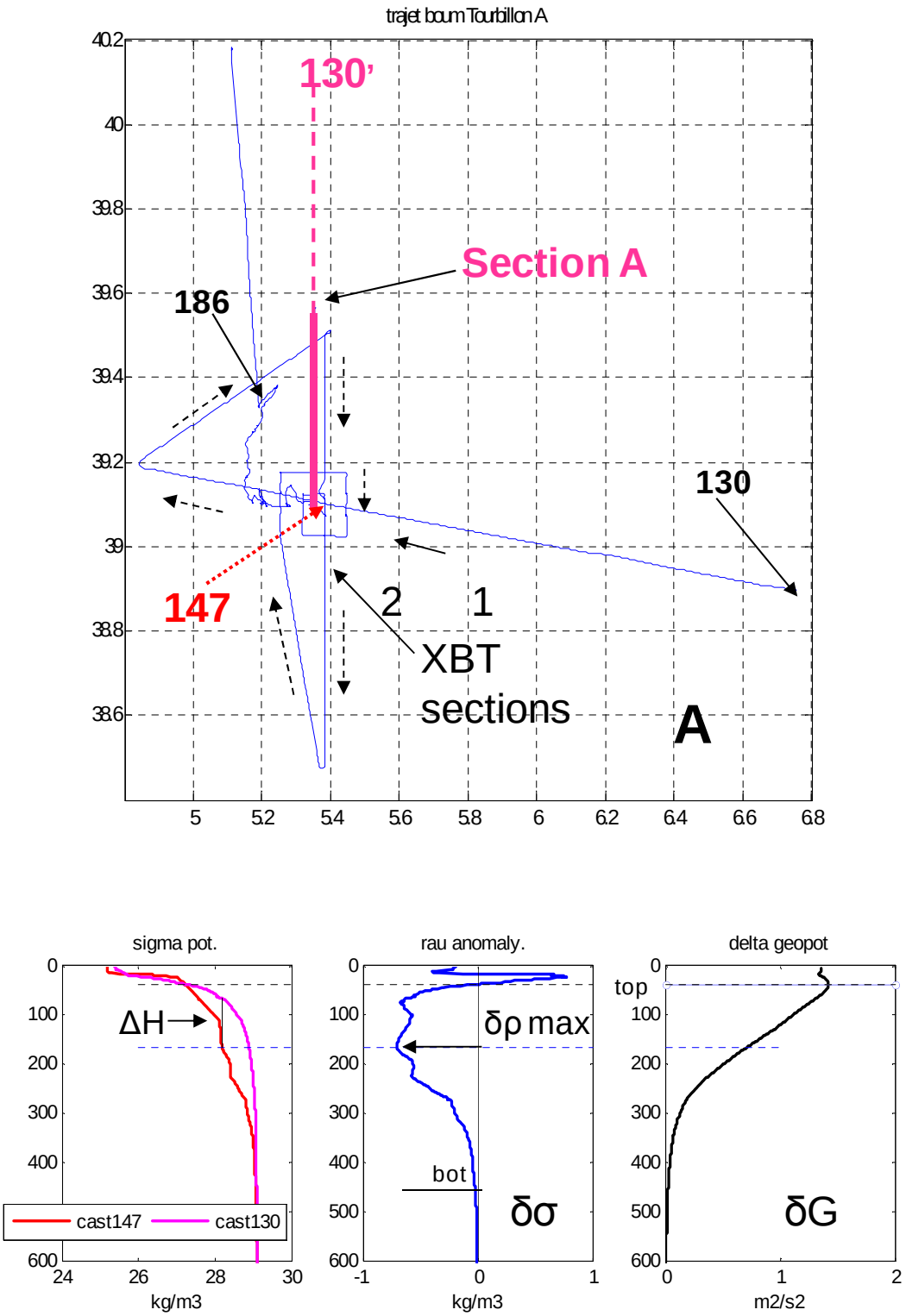

1

2 Fig. SM2 Moutin and Prieur

3

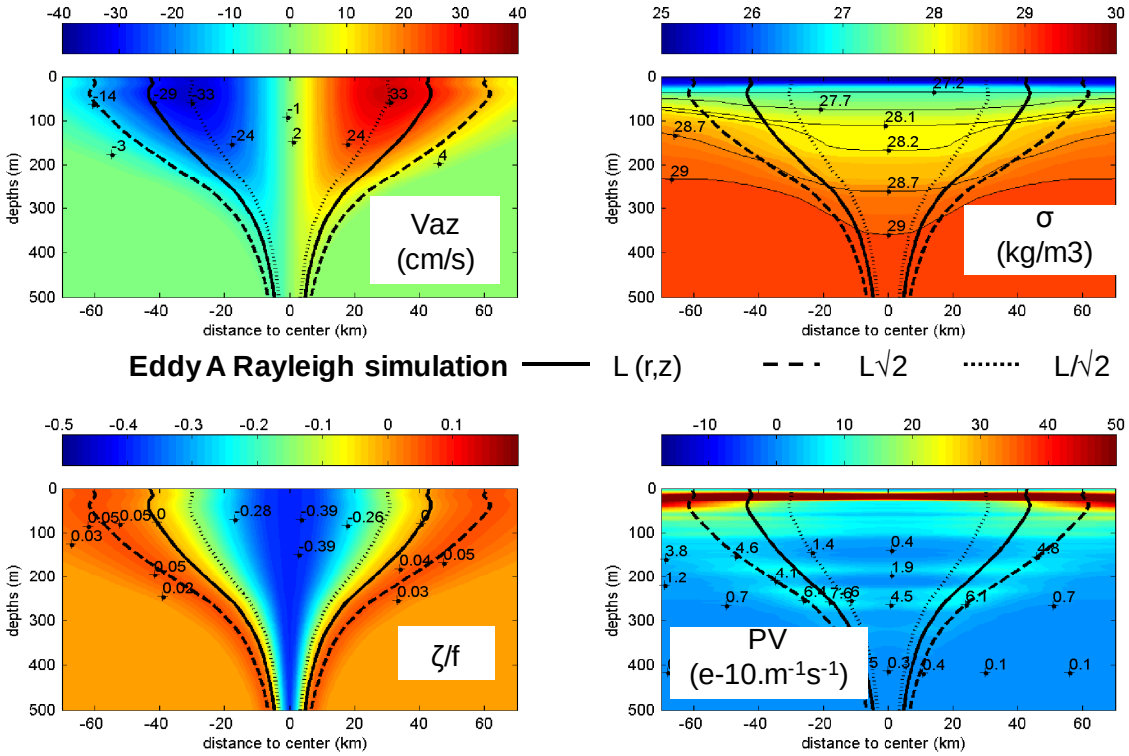

Fig. SM3 Moutin and Prieur

1

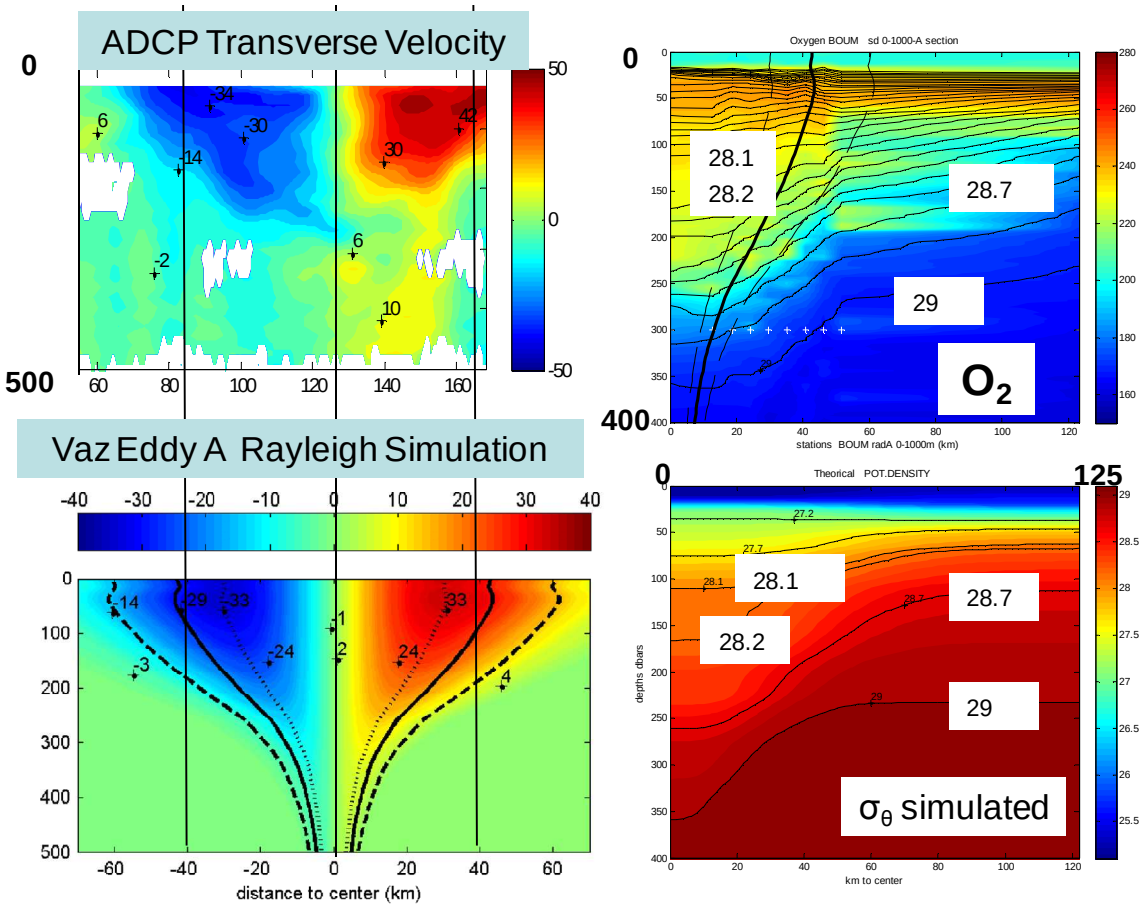

2

3 Fig. SM4 Moutin and Prieur

4